Arrival direction effects of travelling waves on nonlinear seismic response of arch dams

Mehmet Akköse[*]

Department of Civil Engineering, Karadeniz Technical University, 61080, Trabzon, Turkey

Abstract. The aim of this study is to investigate arrival direction effects of travelling waves on non-linear seismic response of arch dams. It is evident that the seismic waves may reach on the dam site from any direction. Therefore, this study considers the seismic waves arrive to the dam site with different angles, $\theta=0^o$, 15°, 30°, 45°, 60°, 75°, and 90° for non-linear analysis of arch dam-water-foundation interaction system. The N-S, E-W and vertical component of the Erzincan earthquake, on March 13, 1992, is used as the ground motion. Dam-water-foundation interaction is defined by Lagrangian approach in which a step-by-step integration technique is employed. The stress-strain behavior of the dam concrete is idealized using three-dimensional Drucker-Prager model based on associated flow rule assumption. The program NONSAP is employed in response calculations. The time-history of crest displacements and stresses of the dam are presented. The results obtained from non-linear analyses are compared with that of linear analyses.

1. Introduction

The non-linear dynamic analysis of concrete dams to earthquake ground motions should be based on a detailed analytical model. Furthermore, this model should be capable of representing correctly both the materially non-linear behavior and a three-dimensional nature of the dam-water-foundation system that account for the interaction effects of the foundation rock and the impounded water (Akpinar *et al.* 2014; Papaleontiou and Tassoulas 2012).

Interaction between the dam and impounded water is an important factor affecting the dynamic response of arch dams during earthquake ground motion. When an arch dam-water system is subjected to a dynamic effect such as earthquake, hydrodynamic pressures in excess of hydrostatic pressures occur on the dam due to the vibration of the dam and water in the reservoir. The importance of the hydrodynamic pressures on the behavior of arch dams subjected to earthquake ground motions has long been recognized (Perumalswami and Kar 1973; Fok and Chopra 1985; Fok and Chopra 1986a, 1986b; Tan and Chopra 1995a, 1995b; Camara 2000; Wang *et al.* 2012; Altunisik and Sesli 2015;). They have shown that the hydrodynamic pressures play an important role on the dynamic response of arch dams.

---

[*]Corresponding author, Associate Professor, E-mail: akkose@ktu.edu.tr

Concrete, capable of displaying non-linear characteristics, is an essential material in many structures such as concrete dams. There are several approaches to model the complicated stress-strain behavior of concrete. In this regard, the theories based on plasticity and fracture mechanics are commonly applied in most of the engineering analysis. However, only few studies taking into account material non-linearity have been performed to investigate the dynamic behavior of concrete arch dams. Kuo (1982) suggested an interface smeared crack approach to model the contraction joints and applied this technique to dynamic analysis of arch dams. Hall (1998) used a simple smeared crack model for modelling the contraction and construction joints. Valliappan *et al*. (1999) utilized a continuum damage mechanics approach to investigate seismic response of arch dams. Espandar and Lotfi (2003) and Lotfi and Samii (2012) compared non-orthogonal smeared crack and an elasto-plastic model based on Mohr-Coulomb yield criterion for dynamic analysis of concrete dams. Akkose *et al*. (2008a; 2008b) also used an elasto-plastic model based on Drucker-Prager yield criterion in the non-linear dynamic analysis of arch dams. In the continuum models, such as elasto-plastic and smeared crack models (Hariri-Ardebili *et al*. 2013), the dam body is assumed as a monolith and the non-linear behavior of the mass concrete of the dam body is investigated.

Different earthquake waves have been recorded in soil surface of each abutment of some dams during the same earthquake (Calciati 1979; Sohrabi-Gilani and Ghaemian 2012). These records show that the earthquake ground motions might be different at different points. This situation also indicates that the seismic waves would arrive different directions on the dam site. Arch dams conduct reactions induced by water pressures on its surface to the foundation rock at their banks by arch effects. Therefore, a nonuniform ground motion can cause relative movement of the abutments of arch dams. This situation can disturb the stability of the arch dams and cause their collapse. In addition, some studies about the subject are available in literature (Szczesiak *et al*. 1999; Maeso *et al*. 2002; Chopra and Wang 2010; Wang and Chopra 2010; Sohrabi-Gilani and Ghaemian 2012). These studies showed that nonuniform excitations can have a significant influence on response of arch dams.

Four earthquake input mechanisms are commonly used in the seismic analysis of dam-foundation rock interaction systems: the standard rigid-base input model, the massless foundation input model, the free-field input model, and the deconvolved base-rock input model (Bayraktar *et al*. 2005). Among these models, the massless-foundation input model is widely used for the linear and non-linear seismic analysis of arch dams (Dowling and Hall 1989; Mays *et al*.,1989; Fok and Chopra 1986; Proulx *et al*. 2001). The massless foundation model assumes that the dam is supported by a large region of deformable and massless rock, which in turn is supported by a rigid base boundary. The seismic input is defined as a history of motion of this rigid base. The wave propagation mechanism does not exist in massless rock. Thus, the ground motions specified at the rigid base are transmitted without modification to the dam–foundation interface. However, this model ignores the radiation damping of semi-unbounded rock (Wang *et al*. 2013).

The aim of this study is to investigate arrival direction effects of travelling waves on non-linear seismic response of arch dams including dam-water-foundation rock interaction. The non-linear dynamic analyses of the selected arch dam are performed according to two assumptions for earthquake ground motion. First, the dam is subjected to uniform ground motion along the dam-foundation interface. In other words, the same ground motion is used for all ground support points or the whole region of contact with the foundations is subjected to the same acceleration simultaneously. Therefore, the massless-foundation input model is considered in the seismic analyses of arch dam-foundation rock interaction systems. Second, it is assumed that the seismic

waves arrive to the dam site with different angles, $\theta=0^{o}$, 15°, 30°, 45°, 60°, 75°, and 90° for non-linear analysis of arch dam-water-foundation interaction system. The N-S, E-W and vertical component of the Erzincan earthquake, on March 13, 1992, is used as the ground motion. Dam-water-foundation interaction is defined by Lagrangian approach in which a step-by-step integration technique is employed. The stress-strain behavior of the dam concrete is idealized using three-dimensional Drucker-Prager model based on associated flow rule assumption. The program NONSAP (1974) is employed in the response calculations. The time-history of crest displacements and stresses on of the dam are presented. The results obtained from non-linear analyses are compared with that of linear analyses.

2. Non-linear material model

Concrete capable of displaying nonlinear characteristics is an essential material in many structures, such as arch dams. The stress-strain curve of concrete depends on many factors. Consequently, defining material behavior correctly is very difficult. For efficient solutions, models representing the behavior of concrete are required. There are many criteria for the determination of yield surface or yield function of materials. Drucker-Prager criterion is widely used for frictional materials such as rock and concrete. Drucker and Prager (1952) obtained a convenient yield function to determine elasto-plastic behaviour of concrete smoothing Mohr-Coulomb criterion. This function is defined as

$$f = \alpha I_1 + \sqrt{J_2} - k \tag{1}$$

where I_1 is the first invariant of stress tensor (σ_{ij}) and J_2 is the second invariant of deviatoric stress tensor (s_{ij}). α and k are constants which depend on cohesion (c) and angle of internal friction (ϕ) of the material given by

$$\alpha = \frac{2\sin\phi}{\sqrt{3}(3-\sin\phi)} \tag{2}$$

$$k = \frac{6c\cos\phi}{\sqrt{3}(3-\sin\phi)} \tag{3}$$

The mid-point integration method is used in the Drucker-Prager model based on associated flow rule assumption. In this integration technique based on two-stepped Runge-Kutta method, first step is called mid-increment step, and second step is called full-increment step.

In the mid-increment step, it is assumed that stresses and strains in an element are σ_{ij}^n and ε_{ij}^n at the end of the n-*th* loading increment, respectively. According to the stress state (elastic or plastic) in the element, either the elastic constitutive matrix (ECM) $\mathbf{D}_e$ or the elasto-plastic constitutive matrix (EPCM) $\mathbf{D}_{ep}$ is used to calculate the current element tangent stiffness. Applying first the half of the incremental loads to the discretized system stiffness $\mathbf{K}^n$, incremental

strains $d\varepsilon_{ij}^{n+1/2}$ at the (n+1/2)-*th* increment are estimated from the kinematic condition as follows

$$d\mathbf{U}^{n+1/2} = (\mathbf{K}^n)^{-1}\left(\frac{1}{2}d\mathbf{R}\right) \text{ in structure level} \tag{4}$$

$$d\boldsymbol{\varepsilon}^{n+1/2} = \mathbf{B}d\mathbf{U}^{n+1/2} \quad \text{in element level} \tag{5}$$

where **U**, **R** and **B** are nodal displacements vector, load vector and strain-displacement matrix, respectively. Subsequently, the corresponding stress increments $d\sigma_{ij}^{n+1/2}$ in all elements are estimated by using the current constitutive matrix $\mathbf{D}_e$ or $\mathbf{D}_{ep}$. Then, the stresses $\sigma_{ij}^{n+1/2}$ for all elements at the end of the (n+1/2)-*th* loading increment are approximated from the stresses σ_{ij}^n

$$d\sigma_{ij}^{n+1/2} = \mathbf{D}_e d\varepsilon_{ij}^{n+1/2} \text{ or } d\sigma_{ij}^{n+1/2} = \mathbf{D}_{ep}^n d\varepsilon_{ij}^{n+1/2} \tag{6}$$

$$\sigma_{ij}^{n+1/2} = \sigma_{ij}^n + d\sigma_{ij}^{n+1/2} \tag{7}$$

The main purpose of the calculation made at the mid-increment step is to correct the stresses $\sigma_{ij}^{n+1/2}$ in all elements if necessary and to construct for each element a new constitutive matrix ($\mathbf{K}^{n+1/2}$).

In the full-increment step, with the aid of the system tangent stiffness $\mathbf{K}^{n+1/2}$ after the (n+1/2)-*th* increment, the (n+1)-*th* incremental calculation is performed to obtain the displacement increment $d\mathbf{U}^{n+1}$ by applying the full load increment $d\mathbf{R}$. Subsequently, the strain increment $d\varepsilon_{ij}^{n+1}$ for the element can be evaluated from the kinematic condition

$$d\mathbf{U}^{n+1} = (\mathbf{K}^{n+1/2})^{-1}d\mathbf{R} \qquad \text{in structure level} \tag{8}$$

$$d\boldsymbol{\varepsilon}^{n+1} = \mathbf{B}d\mathbf{U}^{n+1} \qquad \text{in element level} \tag{9}$$

The stress increment $d\sigma_{ij}^{n+1}$ can be obtained by using the current constitutive matrix $\mathbf{D}_e$ or $\mathbf{D}_{ep}$, and finally the stresses σ_{ij}^{n+1} can be estimated by adding the stress increment $d\sigma_{ij}^{n+1}$ to the stress σ_{ij}^n at the end of the n-th loading increment

$$d\sigma_{ij}^{n+1} = \mathbf{D}_e d\varepsilon_{ij}^{n+1} \text{ or } d\sigma_{ij}^{n+1} = \mathbf{D}_{ep}^{n+1/2} d\varepsilon_{ij}^{n+1} \tag{10}$$

$$\sigma_{ij}^{n+1} = \sigma_{ij}^n + d\sigma_{ij}^{n+1} \tag{11}$$

The mid-point integration method reduces the computational time and provides the necessary accuracy of the solution within the small strain increment. The integration method, which is available in the book written by Chen and Mizuno (1990) in details, was described previously (Akkose *et al*., 2008b). A schematic flow chart prepared for the Drucker-Prager model based on mid-point integration method (Chen and Mizuno, 1990) is shown in Fig. 1.
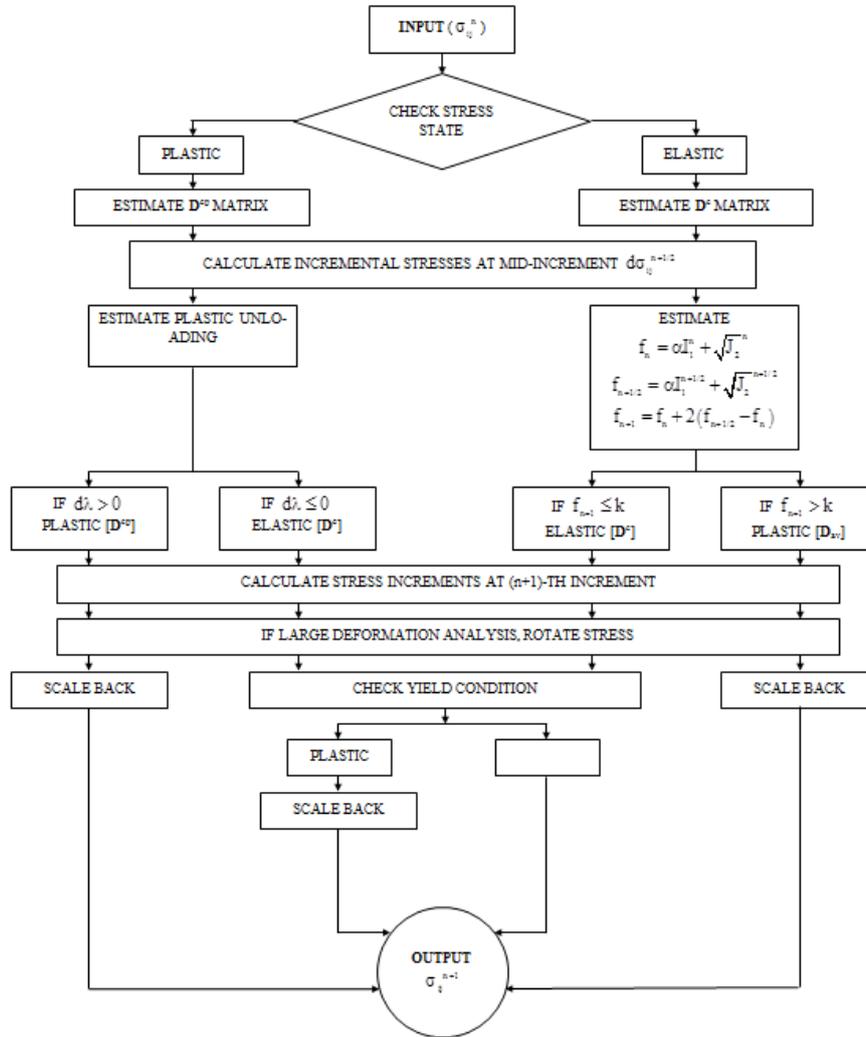
Fig. 1 Flow chart for Drucker-Prager model based on mid-point integration method (Chen and Mizuno, 1990)

3. Lagrangian approach in coupled fluid-structure system

In the Lagrangian approach, fluid is assumed to be linear-elastic, inviscid and irrotational. For a general three-dimensional fluid element, stress-strain relationships can be written in matrix form as follows

$$
\begin{Bmatrix} P \\ P_x \\ P_y \\ P_z \end{Bmatrix} = \begin{bmatrix} C_{11} & 0 & 0 & 0 \\ 0 & C_{22} & 0 & 0 \\ 0 & 0 & C_{33} & 0 \\ 0 & 0 & 0 & C_{44} \end{bmatrix} \begin{Bmatrix} \varepsilon_v \\ w_x \\ w_y \\ w_z \end{Bmatrix} \tag{12}
$$

where P, C_{11}, and ε_v are the pressures which are equal to mean stresses, the bulk modulus and the volumetric strains of the fluid, respectively. Since irrotationality of the fluid is considered like penalty methods (Zienkiewicz and Taylor, 1989; Bathe, 1996), rotations and constraint parameters can be included in the stress-strain equations of the fluid. In Eq. (12), P_x, P_y, P_z are the rotational stresses; C_{22}, C_{33}, C_{44} are the constraint parameters and w_x, w_y and w_z are the rotations about the cartesian axis x, y and z, respectively.

The equations of motion of the fluid system are obtained using energy principles as follows

$$\mathbf{M}_f \ddot{\mathbf{U}}_f + \mathbf{K}_f \mathbf{U}_f + \mathbf{S}_f \mathbf{U}_{sf} = \mathbf{R}_f \tag{13}$$

or

$$\mathbf{M}_f \ddot{\mathbf{U}}_f + \mathbf{K}_f^* \mathbf{U}_f = \mathbf{R}_f \tag{14}$$

where $\mathbf{K}_f^*$, $\ddot{\mathbf{U}}_f$ and $\mathbf{R}_f$ are the system stiffness matrix including the free surface stiffness, the nodal acceleration vector and the time-varying nodal force vector for the fluid system, respectively. In the formation of the fluid element matrices, reduced integration orders are utilized. The 8-noded three-dimensional fluid element is used in the finite element model of the fluid system. For this element, the reduced integration order is (1x1x1).

The equations of motion of the fluid system, Eq. (14), have a similar form to those of the structure system. To obtain the coupled equations of the fluid-structure system, a determination of the interface condition is required. Since the fluid is assumed to be inviscid, only the displacement in the normal direction to the interface is continuous at the interface of the system. Assuming that the positive face is the structure and the negative face is the fluid, the boundary condition at the fluid-structure interface is

$$U_n^- = U_n^+ \tag{15}$$

where U_n is the normal component of the interface displacement (Akkaş *et al.*, 1979). Using the interface condition, the equations of motion of the coupled system to ground motion including damping effects are given by

$$\mathbf{M}_c \ddot{\mathbf{U}}_c + \mathbf{C}_c \dot{\mathbf{U}}_c + \mathbf{K}_c \mathbf{U}_c = -\mathbf{M}_c a_g \tag{16}$$

in which $\mathbf{M}_c$, $\mathbf{C}_c$ and $\mathbf{K}_c$ are the mass, damping and stiffness matrices for the coupled system. $\mathbf{U}_c$ $\dot{\mathbf{U}}_c$ $\ddot{\mathbf{U}}_c$ are the vectors of the displacement, velocity and acceleration of the coupled system. a_g is the vector of ground acceleration. More information about the Lagrangian approach in coupled fluid-structure system can be reached from the references Akkose *et al.* (2008a; 2008b).

4. Numerical application and discussions

4.1 Details of dam-water-foundation rock system

The selected arch dam for this study is Type-5 which was suggested in the symposium on arch dams ICE (1968). The detailed geometrical properties of the Type-5 arch dam can be reached from the references ICE (1968) and Akkose *et al.* (2008a; 2008b). The finite element idealization
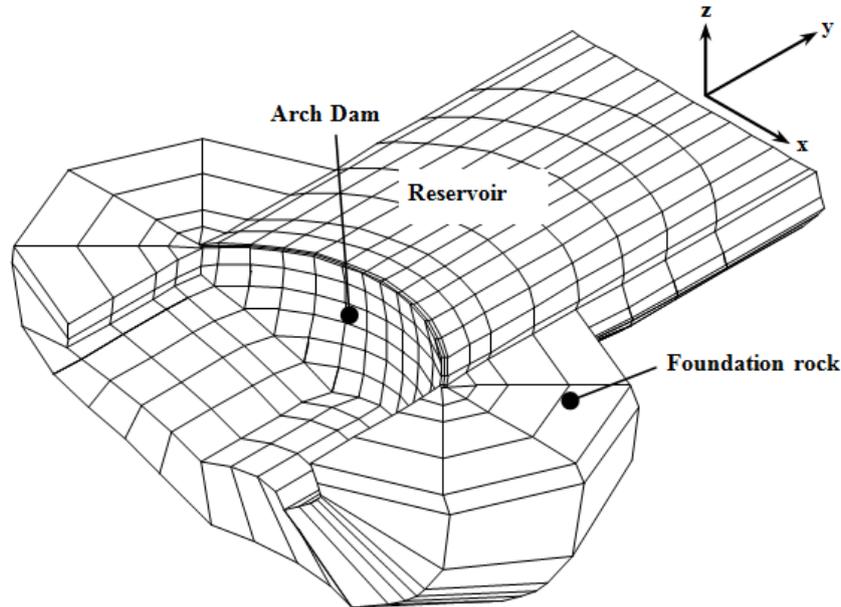
Fig. 2 Axonometric view of arch dam-reservoir-foundation rock interaction system

prepared for dam-water-foundation rock system is presented in Fig. 2.

The depth of reservoir is 120m in the finite element idealization prepared for dam-water-foundation rock system. The reservoir length is selected as three times of the reservoir depth to consider the damping effect arising from the propagation of pressure waves in the upstream direction.

Non-linear behaviour of dam concrete is idealized as elasto-plastic using Drucker-Prager model based on associated flow rule assumption. Elasticity modulus, mass density and Poisson's ratio of the dam concrete are taken as 27579MPa, 2483kg/m^3, and 0,20, respectively. The cohesion (c) and the angle of internal friction (ϕ) for elasto-plastic behaviour of the concrete are 3,75MPa and 35°, respectively. 8-noded three-dimensional solid elements are used to represent the dam. The number of the elements in the dam is 128.

The foundation rock is assumed to be linearly elastic and represented by 8-noded three-dimensional solid elements up to a certain distance from the dam. To avoid reflection of the outgoing waves, these elements are assumed to be massless, and so only its flexibility is included. Elasticity modulus and Poisson's ratio of the foundation rock are taken as 55158MPa and 0,20, respectively. 164 three-dimensional elements are used in the finite element mesh of the foundation rock.

The fluid is assumed to be linearly elastic, inviscid and irrotational. The bulk modulus and mass density of the fluid are taken as 2070MPa and 1000kg/m^3, respectively. The optimum value of the rotation constraint parameters changes with the properties of material and it can be a different value for various problems. The parameters should be as high as necessary to enforce the rotational constraint but small enough to avoid causing numerical ill-conditioning in the assembled stiffness matrix. These parameters of the fluid about each cartesian axes are taken as 1000 times of the bulk modulus in three-dimensional fluid-structure problems due to the mentioned reasons

(Calayır and Dumanoğlu 1993; Hamdan 1999). In addition, 512 eight-noded three-dimensional fluid elements are used to represent the water in the reservoir.

The fluid is only able to transmit normal forces to both solid (canyon sides) and structure (dam) boundaries. This is because of its inviscid nature. The slip condition at the solid-fluid interface can be modelled by the use of constraint relations (Greeves 1991; Calayır *et al.* 1996; Olson and Bathe 1983; Zienkiewicz and Bettes 1978), interface elements (Hamdan 1999) or short and axially almost rigid link (truss) elements in the normal direction of the interface (Akkaş *et al.* 1979). At the interface of the reservoir-canyon, one node, which corresponds to the canyon side, of the link element is completely restrained (grounded) whereas the other is capable of moving in the translational directions. At the interface of the dam-reservoir, each of nodes of the link element allows the translation motions. Thus, complete slip motion between fluid and the canyon and the fluid and the dam is still possible. The length and the elasticity modulus of the truss elements are taken as 0,001m and 2×10^{10}MPa, respectively.

There are 1374 nodal points in the dam-water-foundation rock system (Fig. 2). At the boundaries of the dam-water-foundation rock system, there are 518 restrained degrees of freedom. Hence, the active degrees of freedom (or equations) for dam-water-foundation rock system are determined as 3604 in total.

The Wilson-θ method, which is one of the direct integration methods, is used for the solution of the general equation of motion of the coupled fluid-structure system in this study. The solution time step chosen is 0,001 seconds for the integration. This method requires that the damping matrix to be represented be in explicit form. This is accomplished by using Rayleigh damping (Bathe 1996; Chopra 1995; Clough and Penzien 1993). The damping matrices for the structure are given as follows

$$\mathbf{C}_s = a_0\mathbf{M}_s + a_1\mathbf{K}_s \qquad (17)$$
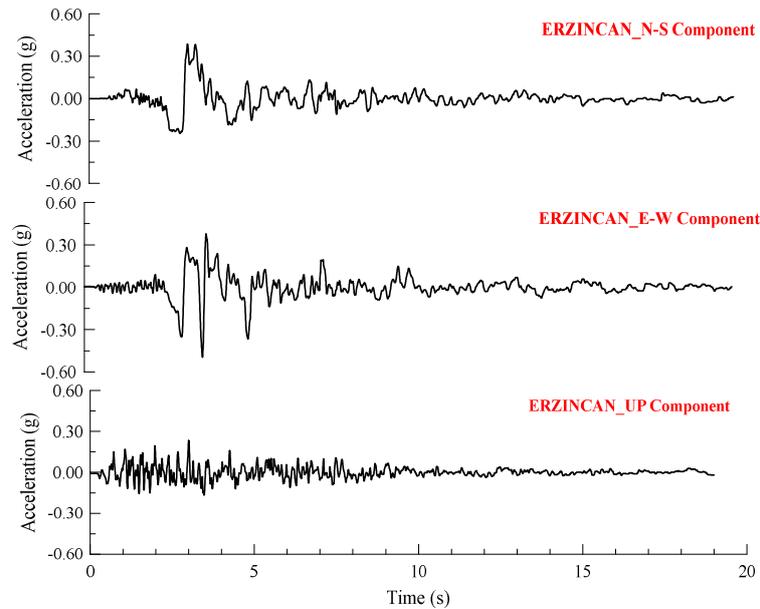
Fig. 3 The E-W, N-S and vertical components of Erzincan earthquake, on March 13, 1992 (PEER, 2015)
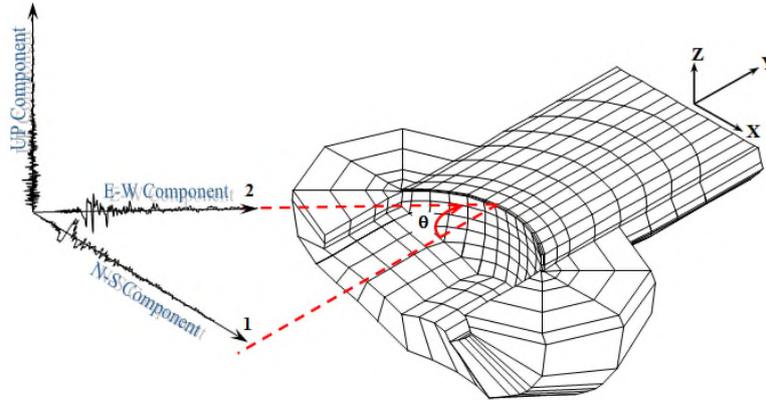
Fig. 4 The depiction of seismic waves arriving to the dam site with different angles

where coefficients a_0 and a_1 obtained from two given damping ratios associated with two frequencies of vibration. If both frequencies are assumed to have the same damping ratio (ξ), then a_0 and a_1 constants can be obtained by (Bathe 1996; Chopra 1995; Clough and Penzien 1993)

$$a_0 = \xi \frac{2\omega_i\omega_j}{\omega_i + \omega_j} \text{ and } a_1 = \xi \frac{2}{\omega_i + \omega_j} \tag{18}$$

where ω_i ve ω_j are the ith and jth mode frequencies of the system, respectively. The damping constants are calculated within frequency range 2 to 15 Hz of the natural frequency of the first bending mode for the dam-water-foundation rock system assuming 5% damping ratio. The first frequency of the system is 2,941Hz. Accordingly, this frequency range ensures the damping ratio.

In the earthquake analysis of a dam, the displacements and stresses due to static loads should be included in the total responses. However, the static effects are not included in the results presented here because they can complicate the interpretation of both simultaneous effects of three components of an earthquake on the seismic response of arch dams and arrival direction effects of travelling waves on non-linear seismic response of arch dams as expressed by Fok and Chopra (1985).

4.2 Earthquake ground motion

The Erzincan earthquake, on March 13, 1992 is chosen as the ground motion (PEER, 2015) for non-linear dynamic analyses of the selected arch dam. The E-W, N-S and vertical components of the earthquake are given in Fig. 3.

In this study, non-linear dynamic analyses of the selected arch dam are performed according to two assumptions for earthquake ground motion. First, the dam is subjected to uniform ground motion along the dam-foundation interface. In other words, the same ground motion is used for all ground support points or the whole region of contact with the foundations is subjected to the same acceleration simultaneously. Second, the seismic waves arrive to the dam site with different angles. This situation is depicted in Fig. 4. In the analyses, the arch dam is subjected to the E-W, N-S and vertical components of the earthquake, simultaneously. Since the selected earthquake ground
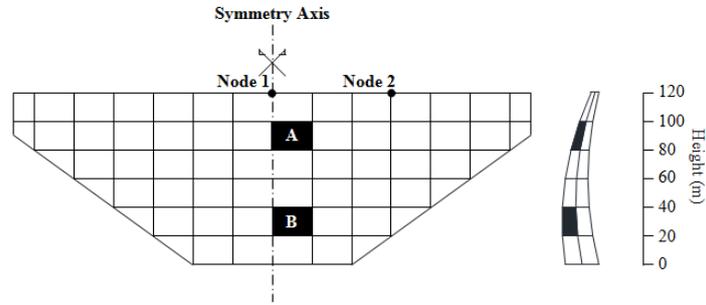
Fig. 5 The upstream view and crown cantilever section of Type-5 arch dam body
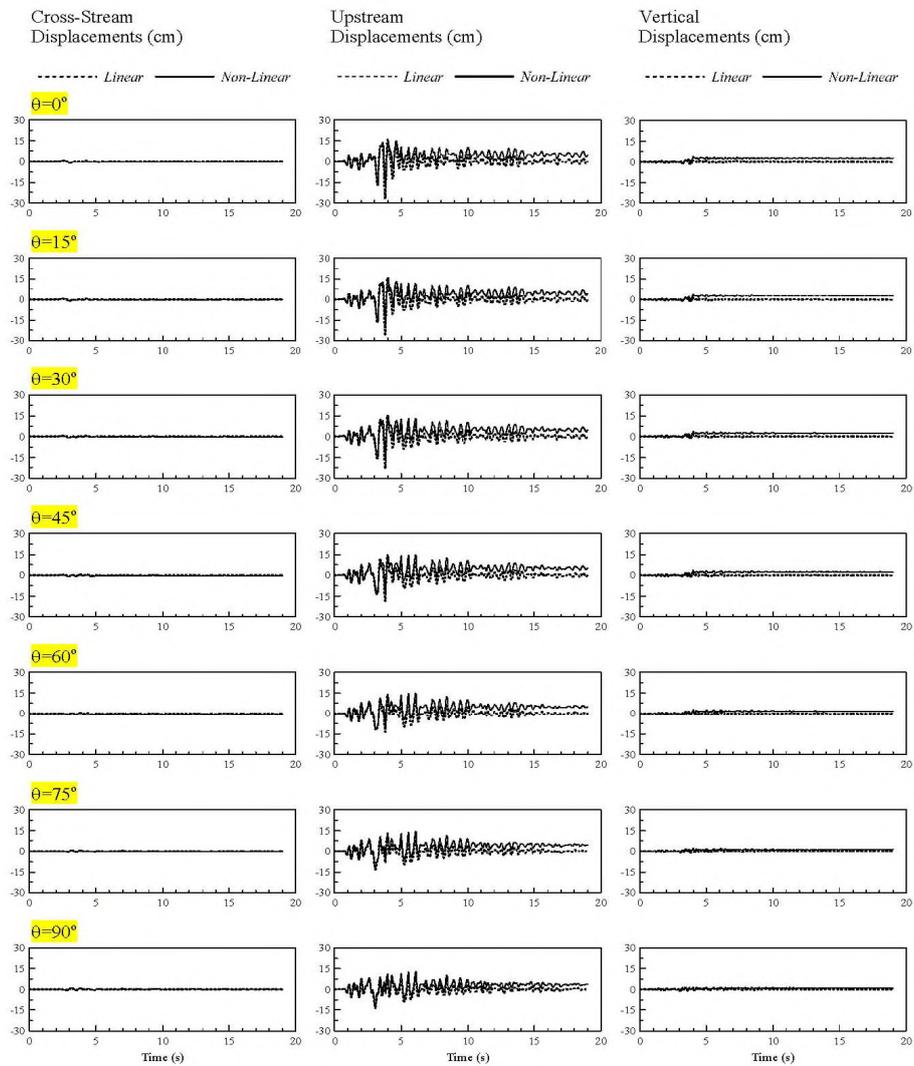
Fig. 6 The time-history of crest displacements at the Node 1 of the arch dam due to simultaneous effect of E-W, N-S and vertical components of Erzincan earthquake (θ = 0°, 15°, 30°, 45°, 60°, 75°, and 90°)

motion can be applied to the dam site with different angles, its components are transformed to the X-Y-Z global coordinate system using the following equation (Khaled *et al.* 2006)

$$\begin{Bmatrix} \ddot{u}_x(t) \\ \ddot{u}_y(t) \end{Bmatrix} = \begin{bmatrix} \cos\theta & -\sin\theta \\ \sin\theta & \cos\theta \end{bmatrix} \begin{Bmatrix} \ddot{u}_1(t) \\ \ddot{u}_2(t) \end{Bmatrix}$$

(19)
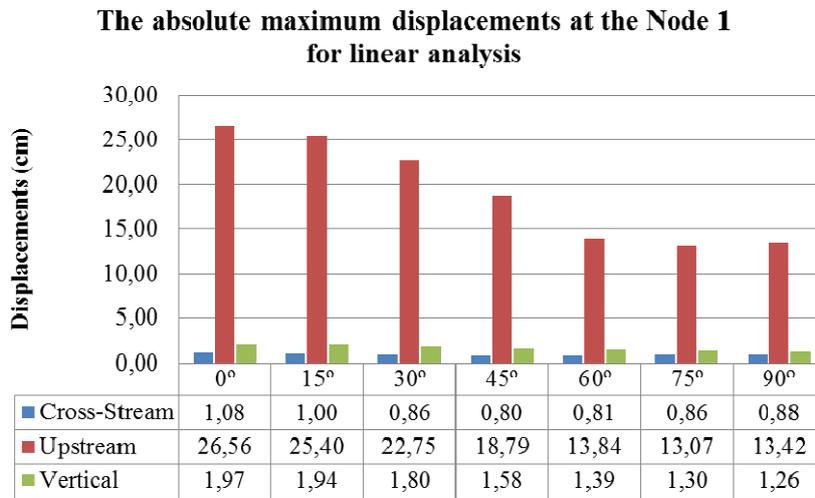
The absolute maximum displacements at the Node 1 for linear analysis

	0°	15°	30°	45°	60°	75°	90°
Cross-Stream	1,08	1,00	0,86	0,80	0,81	0,86	0,88
Upstream	26,56	25,40	22,75	18,79	13,84	13,07	13,42
Vertical	1,97	1,94	1,80	1,58	1,39	1,30	1,26

Fig. 7 The absolute maximum crest displacements at the Node 1 for linear analyses

The absolute maximum displacements at the Node 1 for non-lincar analysis

	0°	15°	30°	45°	60°	75°	90°
Cross-Stream	1,11	1,05	0,93	0,86	0,88	0,85	0,78
Upstream	18,33	18,15	16,92	14,61	14,92	14,18	13,02
Vertical	3,73	3,78	3,62	3,32	2,78	2,16	1,75
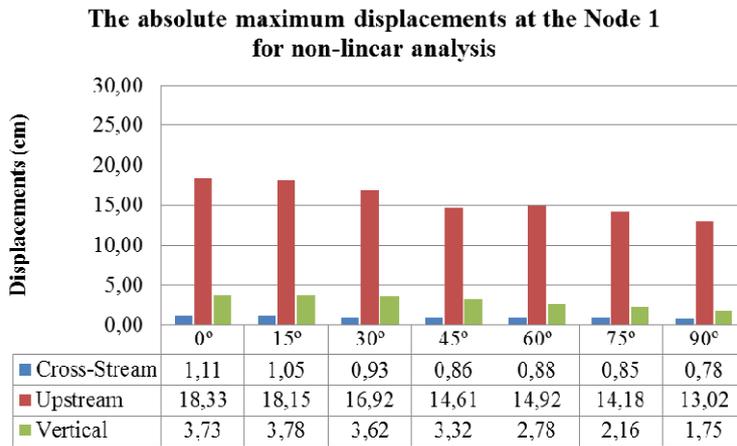
Fig. 8 The absolute maximum crest displacements at the Node 1 for non-linear analyses

4.3 Response results

Non-linear seismic responses of the selected arch dam due to simultaneous effect of E-W, N-S and vertical components of Erzincan earthquake are obtained for different arrival directions of the
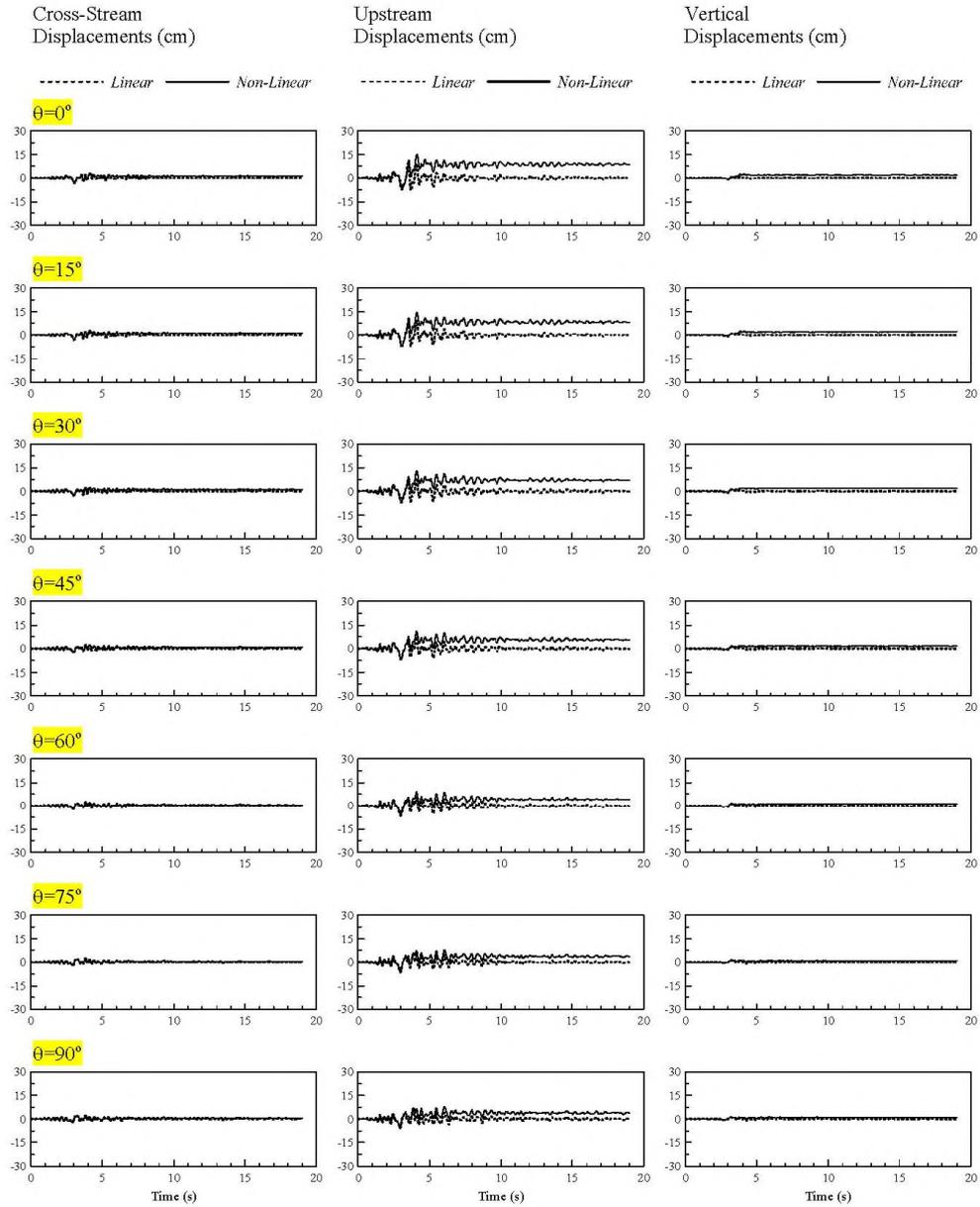
Fig. 9 The time-history of crest displacements at the Node 2 of the arch dam due to simultaneous effect
of E-W, N-S and vertical components of Erzincan earthquake (θ = 0°, 15°, 30°, 45°, 60°, 75°, and 90°)

travelling waves to the dam site. The directions are defined by angles θ=0°, 15°, 30°, 45°, 60°, 75°,
and 90°. The θ angle is measured from the symmetry axis of the dam (Y-Z plane in Fig. 4).

The response results selected in this study consist of the time-history of displacements of some
nodes at crest and of stresses at some elements on dam body. These nodes and elements is shown
in Fig. 5.

4.3.1 Displacements

The time-histories of crest displacements at the node 1, which is on the symmetric axis and also on crown cantilever section, of the selected arch dam due to three component of Erzincan earthquake ground motion acting simultaneously are shown in Fig. 6 for different arrival directions of the travelling waves to the dam site (θ=0°, 15°, 30°, 45°, 60°, 75°, and 90°). The absolute maximum horizontal crest displacements of the dam for linear and non-linear analyses are also compared in Figs. 7 and 8. With the arrival angles of the travelling waves to the dam site increasing from 0° to 90°, the absolute maximum crest displacement decreases from 1,08 to 0,88cm at the cross-stream direction, from 26,56 to 13,42cm at the upstream direction and from
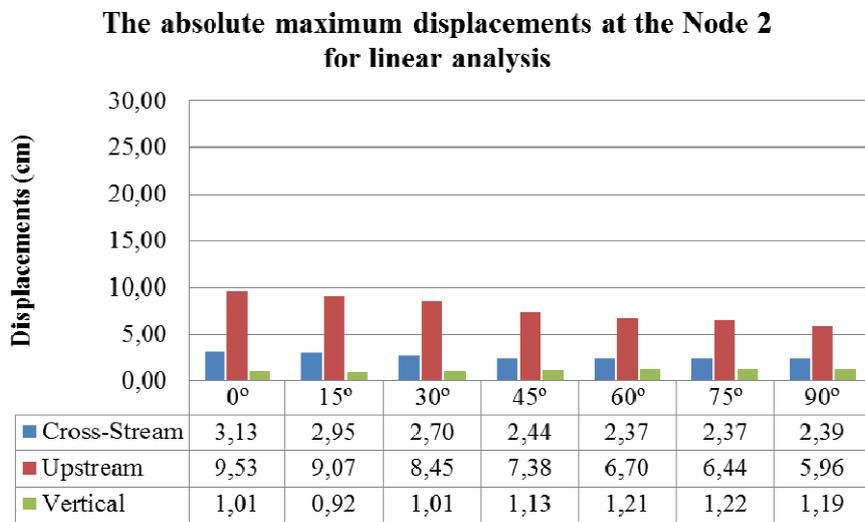
The absolute maximum displacements at the Node 2 for linear analysis

	0°	15°	30°	45°	60°	75°	90°
Cross-Stream	3,13	2,95	2,70	2,44	2,37	2,37	2,39
Upstream	9,53	9,07	8,45	7,38	6,70	6,44	5,96
Vertical	1,01	0,92	1,01	1,13	1,21	1,22	1,19

Fig. 10 The absolute maximum crest displacements at the Node 2 for linear analyses

The absolute maximum displacements at the Node 2 for non-linear analysis

	0°	15°	30°	45°	60°	75°	90°
Cross-Stream	3,18	3,00	2,76	2,52	2,37	2,36	2,38
Upstream	14,70	14,24	12,93	11,00	8,75	7,78	7,85
Vertical	2,37	2,43	2,25	1,88	1,59	1,52	1,39
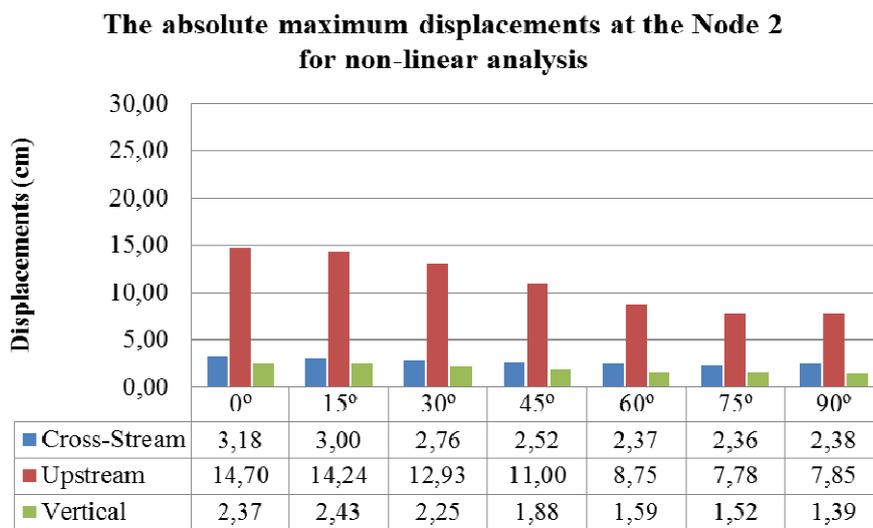
Fig. 11 The absolute maximum crest displacements at the Node 2 for non-linear analyses

1,97 to 1,26cm at the vertical direction for linear analysis (Fig. 7). In the same way, with the arrival angles of the travelling waves to the dam site increasing from 0° to 90°, the absolute maximum crest displacement decreases from 1,11 to 0,78cm at the cross-stream direction, from 18,33 to 13,02cm at the upstream direction and from 3,73 to 1,75cm at the vertical direction for non-linear analysis (Fig. 8).

The time-history of crest displacements at the node 2 of the selected arch dam due to three component of Erzincan earthquake ground motion acting simultaneously are shown in Fig. 9 for
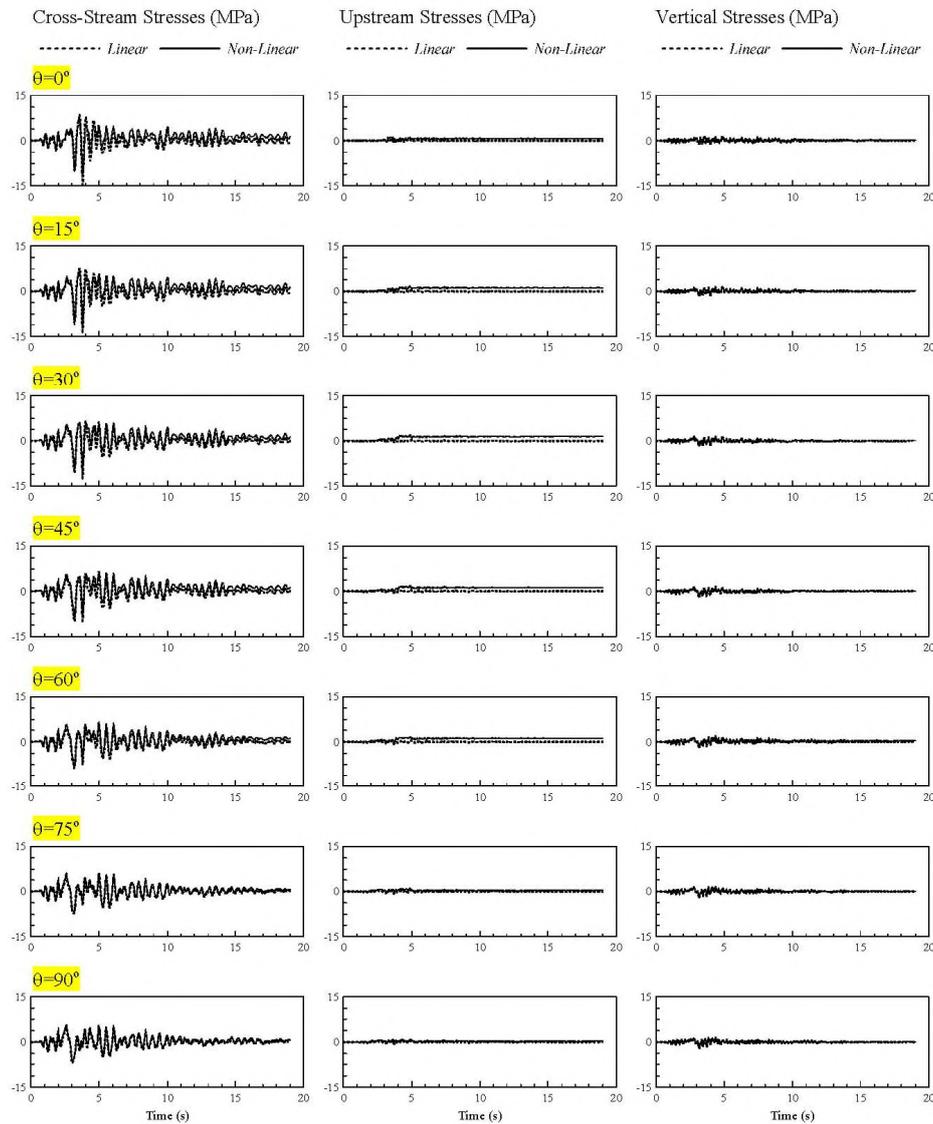
Fig. 12 The time-history of stresses at the element A of the arch dam due to simultaneous effect of E-W, N-S and vertical components of Erzincan earthquake ($\theta = 0^o$, 15°, 30°, 45°, 60°, 75°, and 90°)

The absolute maximum stresses at the element A for linear analysis

	0º	15º	30º	45º	60º	75º	90º
Cross-Stream	14,50	13,87	12,46	10,35	8,68	7,27	6,95
Upstream	0,52	0,53	0,58	0,63	0,65	0,64	0,63
Vertical	1,26	1,53	1,77	1,95	2,07	2,12	2,09
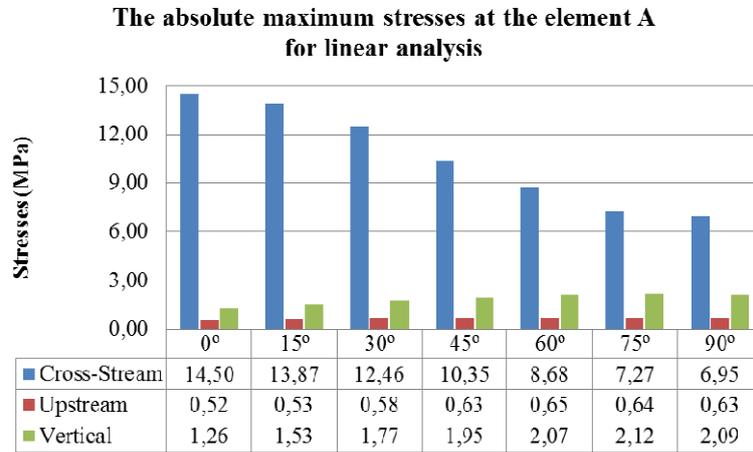
Fig. 13 The absolute maximum stresses at the elements A of Type-5 arch dam for linear analyses

different arrival directions of the travelling waves to the dam site ($\theta = 0^o$, 15°, 30°, 45°, 60°, 75°, and 90°). The absolute maximum horizontal crest displacements of the dam for linear and non-linear analyses are also compared in Figs. 10 and 11. With the arrival angles of the travelling waves to the dam site increasing from 0° to 90°, the absolute maximum crest displacements decrease from 3,13 to 2,39cm at the cross-stream direction and from 9,53 to 5,96cm at the upstream direction. In contrast to displacements at the cross-stream and upstream directions, the absolute maximum crest displacements at the vertical direction increase from 1,01 to 1,19cm for linear analysis (Fig. 10).

With the arrival angles of the travelling waves to the dam site increasing from 0° to 90°, the absolute maximum crest displacements decrease from 3,18 to 2,38cm at the cross-stream direction, from 14,70 to 7,85cm at the upstream direction and from 2,37 to 1,39cm at the vertical direction for non-linear analysis (Fig. 11).

The absolute maximum stresses at the element A for non-linear analysis

	0º	15º	30º	45º	60º	75º	90º
Cross-Stream	11,69	11,33	10,16	9,18	8,08	6,77	6,64
Upstream	1,16	1,60	1,95	1,91	1,75	1,06	0,79
Vertical	1,40	1,52	1,63	1,87	2,03	2,02	1,90
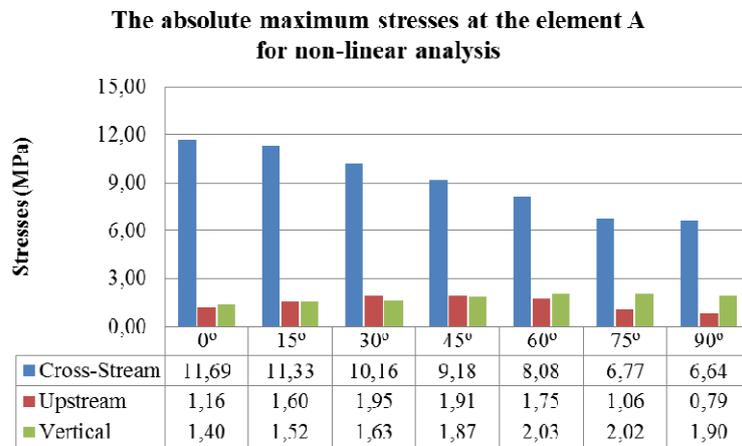
Fig. 14 The absolute maximum stresses at the elements A of Type-5 arch dam for non-linear analyses
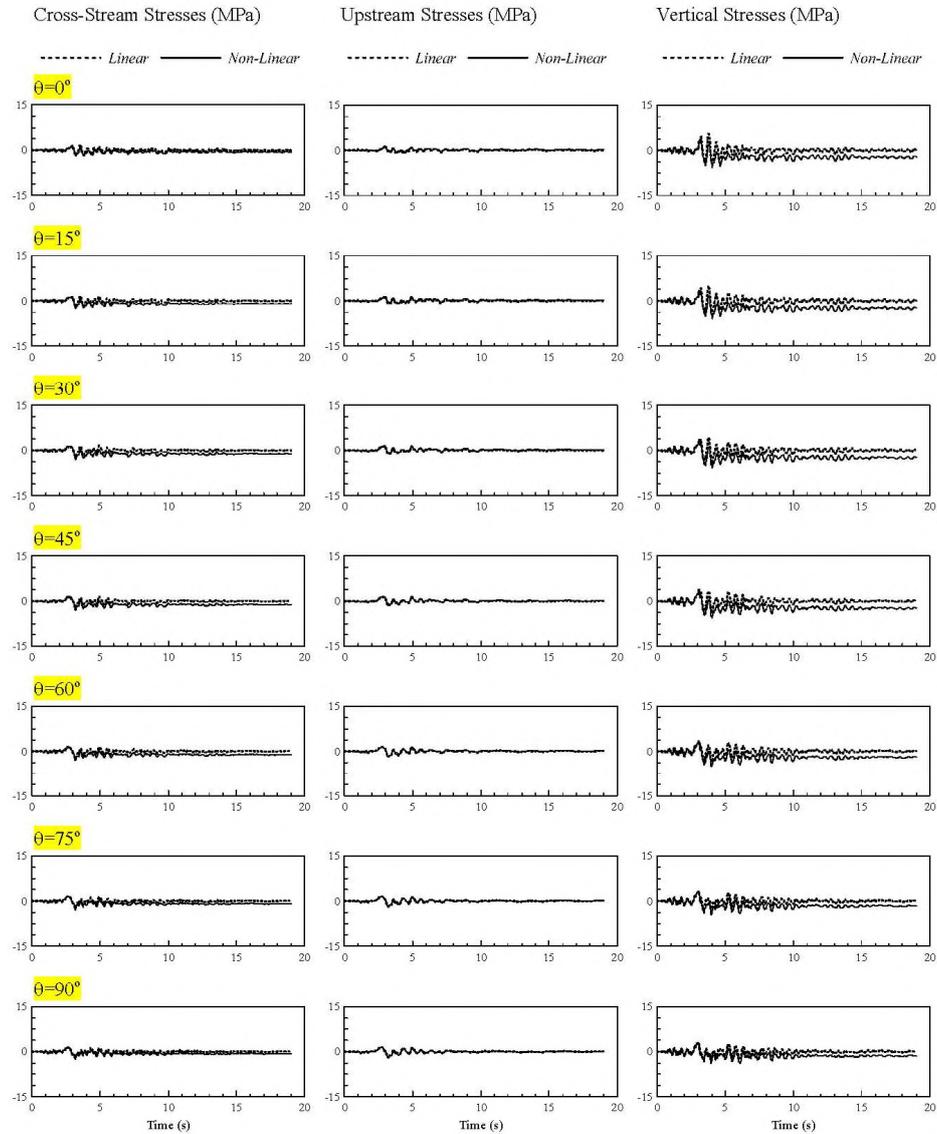
Fig. 15 The time-history of stresses at the element B of the arch dam due to simultaneous effect of E-W, N-S and vertical components of Erzincan earthquake (θ = 0°, 15°, 30°, 45°, 60°, 75°, and 90°)

Comparison of the displacement results obtained from linear and non-linear analyses of the arch dam shows a drift in the crest displacements. It is pointed out that this drift response is the main characteristic of the time-history of displacements in the elasto-plastic analyses because of extensive tensile stresses on the dam body. The major source of the drift response is the cumulative strain that occurs when the stress state exceeds the apex of the failure or yield surface due to the tensile stresses (Akkose *et al*. 2008a; 2008b). As expected, the greatest displacements

occurred at the upstream direction, not at the cross-stream or vertical direction, for both linear and non-linear analysis. Also, crest displacements at the Node 1 are greater than that at the Node 2. This is because of decreasing the flexibility of the arch dam from the crown cantilever section to abutments.

4.3.2 Stresses

The time-history of stresses at the element A on dam body due to three component of Erzincan earthquake ground motion acting simultaneously are shown in Fig. 12 for different arrival directions of the travelling waves to the dam site ($\theta=0^o$, 15°, 30°, 45°, 60°, 75°, and 90°). The absolute maximum stresses at element A in the dam body for linear and non-linear analyses are also compared in Figs. 13 and 14. With the arrival angles of the travelling waves to the dam site increasing from 0° to 90°, the absolute maximum stresses at the element A decrease from 14,50 to 6,95 MPa at the cross-stream direction. In contrast to stresses at the cross-stream direction, the absolute maximum stresses increase from 0,52 to 0,63 MPa at the upstream direction and from 1,26 to 2,09 MPa at the vertical direction for linear analysis (Fig. 13). With the arrival angles of the travelling waves to the dam site increasing from 0° to 90°, the absolute maximum stresses decrease from 11,69 to 6,64 MPa at the cross-stream direction and from 1,16 to 0,79 MPa at the upstream direction. In contrast to stresses at the cross-stream and upstream directions, the absolute maximum stresses at the vertical direction increase from 1,40 to 1,90 MPa for non-linear analysis (Fig. 14).

The time-history of stresses at the element B on dam body due to three component of Erzincan earthquake ground motion acting simultaneously are shown in Fig. 15 for different arrival directions of the travelling waves to the dam site ($\theta=0^o$, 15°, 30°, 45°, 60°, 75°, and 90°). The absolute maximum stresses at element A in the dam body for linear and non-linear analyses are also compared in Figs. 16-17. With the arrival angles of the travelling waves to the dam site increasing from 0° to 90°, the absolute maximum stresses at the element B increase from 1,81 to 2,12 MPa at the cross-stream direction and from 1,50 to 2,06 MPa at the upstream direction. In
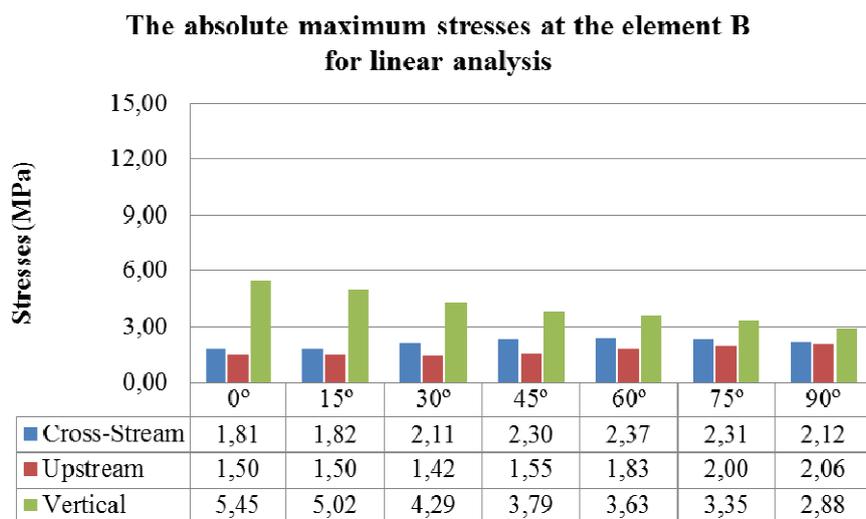
The absolute maximum stresses at the element B for linear analysis

	0°	15°	30°	45°	60°	75°	90°
Cross-Stream	1,81	1,82	2,11	2,30	2,37	2,31	2,12
Upstream	1,50	1,50	1,42	1,55	1,83	2,00	2,06
Vertical	5,45	5,02	4,29	3,79	3,63	3,35	2,88

Fig. 16 The absolute maximum stresses at the elements B of Type-5 arch dam for linear analyses

**The absolute maximum stresses at the element B
for non-linear analysis**

	0°	15°	30°	45°	60°	75°	90°
■ Cross-Stream	1,95	2,54	2,93	3,07	3,03	2,84	2,49
■ Upstream	1,51	1,53	1,49	1,48	1,73	1,96	2,09
■ Vertical	5,65	5,91	5,90	5,54	4,99	4,54	3,90
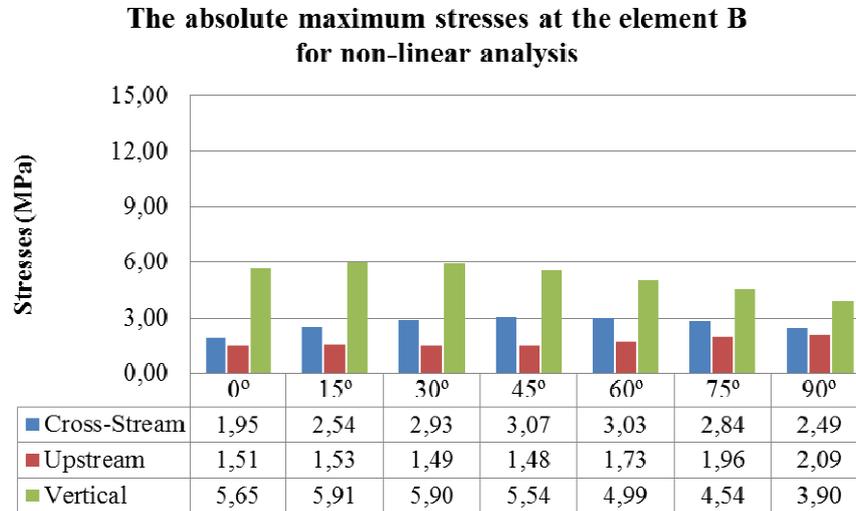
Fig. 17 The absolute maximum stresses at the elements B of Type-5 arch dam for non-linear analyses

contrast to stresses at the cross-stream and upstream directions, the absolute maximum stresses the vertical direction decrease from 5,45 to 2,88 MPa for linear analysis (Fig. 16). With the arrival angles of the travelling waves to the dam site increasing from 0° to 90°, the absolute maximum stresses increase from 1,95 to 2,49 MPa at the cross-stream direction and from 1,51 to 2,09 MPa at the upstream direction. In contrast to stresses at the cross-stream and upstream directions, the absolute maximum stresses at the vertical direction decrease from 5,65 to 3,90 MPa for non-linear analysis (Fig. 17).

As in the crest displacements, the drift response is also seen in the stresses. The arch action in the response of the arch dam is quite pronounced. The stresses in the element A quite good reflect this action. The cross-stream stresses in the element A are the clearest indicator of this action. It is seen from the Fig. 12 that cross-stream stresses in the element A are greater than upstream and vertical stresses for both linear and non-linear analysis. However, vertical stresses in the element B are greater than upstream and cross-stream stresses for both linear and non-linear analysis (Fig. 15). This is the clearest indicator of cantilever action at the arch dam. In addition, the relative significance of arch and cantilever actions varies with the geometry of the dam.

5. Conclusions

In this study, arrival direction effects of travelling waves on non-linear seismic response of arch dams are investigated. Therefore, it is considered that the seismic waves arrive to the dam site with different angles $\theta=0^o$, 15°, 30°, 45°, 60°, 75°, and 90° for non-linear analysis of arch dam-water-foundation interaction systems. The results obtained from non-linear analyses of the arch dam for the different arrival angles of the selected ground motion are compared with linear results.

As expected, the greatest displacements occurred at the upstream direction, not at the cross-stream or vertical direction, for both linear and non-linear analyses. Also, the crest displacements

decrease due to decreasing the flexibility of the arch dam from the crown cantilever section to abutments. With the arrival angles of the travelling waves to the dam site increasing from 0° to 90°, the absolute maximum crest displacement decreases at the cross-stream, upstream and vertical directions for both linear and non-linear analyses.

With the arrival angles of the travelling waves to the dam site increasing from 0° to 90°, the absolute maximum stresses at the element A, in which the arch action is quite prominent in the response of the arch dam, decrease at the cross-stream direction for linear analysis. In contrast to stresses at the cross-stream direction, they increase at the upstream and vertical directions. However, the absolute maximum stresses decrease at the cross-stream and upstream directions whereas they increase at the vertical direction for non-linear analysis.

With the arrival angles of the travelling waves to the dam site increasing from 0° to 90°, the absolute maximum stresses at the element B, in which the cantilever action is quite prominent in the response of the arch dam increase at the cross-stream and upstream directions for linear analysis. In contrast to stresses at the cross-stream and upstream directions, the absolute maximum stresses at decrease at the vertical direction. However, the absolute maximum stresses increase at the cross-stream and upstream directions for non-linear analysis. In contrast to stresses at the cross-stream and upstream directions, they decrease at the vertical direction.

The arch action in the response of the arch dam is quite pronounced. The stresses in the element A well reflects this action. The cross-stream stresses in the element A are the clearest indicator of this action. It is seen from the results that cross-stream stresses in the element A are greater than upstream and vertical stresses for both linear and non-linear analyses. However, vertical stresses in the element B are greater than upstream and cross-stream stresses for both linear and non-linear analyses. This is the clearest indicator of cantilever action at the arch dam. In addition, the relative significance of arch and cantilever actions varies with the geometry of the dam.

It can be said that the linear and non-linear dynamic response of arch dams to the earthquake ground motion is affected from several factors including interaction of the dam with the foundation rock and reservoir water, computer modelling and material properties used in the analysis. In the light of the conclusions of this study, arrival direction effects of travelling waves should be added to these factors.

References

Akkas, N., Akay, H.U. and Yilmaz, C. (1979), "Applicability of general-purpose finite element programs in solid-fluid interaction problems", *Comput. Struct.*, **10**(5), 773-783.

Akköse, M., Adanur, S., Bayraktar, A. and Dumanoğlu, A.A. (2008), "Elasto-plastic earthquake response of arch dams including fluid–structure interaction by the Lagrangian approach", *Appl. Math. Model.*, **32**(11), 2396-2412.

Akkose, M., Bayraktar, A. and Dumanoglu, A.A. (2008), "Reservoir water level effects on nonlinear dynamic response of arch dams", *J. Fluid. Struct.*, **24**(3), 418-435.

Akpinar, U., Binici, B. and Arici, Y. (2014), "Earthquake stresses and effective damping in concrete gravity dams", *Earthq. Struct.*, **6**(3), 251-266.

Altunisik, A.C. and Sesli, H. (2015), "Dynamic response of concrete gravity dams using different water modelling approaches: westergaard, lagrange and euler", *Comput. Concrete*, **16**(3), 429-448.

Bathe, K.J. (1996), *Finite element procedures in engineering analysis*, Prentice-Hall, Englewood Cliffs, New Jersey.

Bathe, K.J., Wilson, E.L. and Iding, R. (1974), "NONSAP: A structural analysis program for static and

dynamic response of nonlinear systems", *Struct. Eng. Struct. Mech.*, Department of Civil Engineering, Report No. UC SESM 74-3, *University of California*, Berkeley, California.

Bayraktar, A., Hançer, E. and Akköse, M. (2005), "Influence of base-rock characteristics on the stochastic dynamic response of dam–reservoir–foundation systems", *Eng. Struct*, **27**(10), 1498-1508.

Calayir, Y. and Dumanoğlu, A.A. (1993), "Static and dynamic analysis of fluid and fluid-structure systems by the Lagrangian method", *Comput. Struct.*, **49**(4), 625-632.

Calayir, Y., Dumanoğlu, A.A. and Bayraktar, A. (1996), "Earthquake analysis of gravity dam-reservoir systems using the Eulerian and Lagrangian approaches", *Comput. Struct.*, **59**(5), 877-890.

Calciati, F., Castoldi, A., Ciacci, R. and Fanelli, M. (1979), "Experience gained during in situ artificial and natural dynamic excitation of large concrete dams in Italy", Analytical interpretation of results, Trans. COLD Congress, New Delhi, **4**, Q51, R32.

Camara, R.J. (2000), "A method for coupled arch dam-foundation-reservoir seismic behaviour analysis", *Earthq. Eng. Struct. Dy.*, **29**(4), 441-460.

Chen, W.F. and Mizuno, E. (1990), *Nonlinear analysis in soil mechanics*, Elsevier Science Publishers B. V., Amsterdam, Netherlands.

Chopra, A.K. (1995), *Dynamics of structures*, Prentice-Hall, New Jersey, USA.

Chopra, A.K. and Wang, J.T. (2010), "Earthquake response of arch dams to spatially varying ground motion", *Earthq. Eng. Struct. Dy.*, **39**(8), 887-906.

Clough, R.W., and Penzien, J. (1993), *Dynamics of Structures*, Second Edition, McGraw-Hill Book Company, Singapore.

Dowling, M.J. and Hall, J.F. (1989), "Nonlinear seismic analysis of arch dams", *J. Eng. Mech.*, **115**(4), 768-789.

Drucker, D.C. and Prager, W. (1952), "Soil mechanics and plastic analysis on limit design", *Q. J. Appl. Math.*, **10**(2), 157-165.

Espandar, R. and Lotfi, V. (2003), "Comparison of non-orthogonal smeared crack and plasticity models for dynamic analysis of concrete arch dams", *Comput. Struct.*, **81**(14), 1461-1474.

Fok, K.L. and Chopra, A.K. (1986), "Earthquake analysis of arch dams including dam–water interaction, reservoir boundary absorption and foundation flexibility", *Earthq. Eng. Struct. Dy.*, **14**(2), 155-184.

Fok, K.L. and Chopra, A.K. (1986), "Hydrodynamic and foundation flexibility effects in earthquake response of arch dams", *J. Struct. Eng.*, **112**(8), 1810-1828.

Fok, K.L., and Chopra, A.K. (1985), "Earthquake analysis and response of concrete arch dams", Earthquake Engineering Research Center Report No. UCB/EERC-85/07, University of California, Berkeley, California.

Greeves, E.J. (1991), "The modelling and analysis of linear and nonlinear fluid-structure systems with particular reference to concrete dams", Ph.D. Thesis, Department of Civil Engineering, *University of Bristol*.

Hall, J.F. (1998), "Efficient non-linear seismic analysis of arch dams", *Earthq. Eng. Struct. Dy.*, **27**(12), 1425-1444.

Hamdan, F.H. (1999), "Near-field fluid–structure interaction using Lagrangian fluid finite elements", *Comput. Struct.*, **71**(2), 123-141.

Hariri-Ardebili, M.A., Seyed-Kolbadi, S.M. and Mirzabozorg, H. (2013), "A smeared crack model for seismic failure analysis of concrete gravity dams considering fracture energy effects", *Struct. Eng. Mech.*, **48**(1), 17-39.

ICE (1968), "Arch dams: A review of British research and development", *Proceedings of the Symposium Held at the Institution of Civil Engineers*, 20-21 March, London, England.

Khaled, A., Tremblay R. and Massicotte, B. (2006), "Assessing the adecuacy of the 30% combination rule in estimating the critical response of bridge piers under multi-directional earthquake components", *Proceedings of the 7th International Conference on Short&Medium Span Bridges*, Paper No. SD-014-1, Monreal, Canada.

Kuo, J.S.H. (1982), "Joint opening nonlinear mechanism: interface smeared crack model", Earthquake

Engineering Research Center, Report No. UCB/EERC-82/10, *University of California*, Berkeley, California, 1982.

Lotfi, V. and Samii, A. (2012), "Dynamic analysis of concrete gravity dam-reservoir systems by wavenumber approach in the frequency domain", *Eartq. Struct.*, **3**(3), 533-548.

Maeso, O., Aznarez, J.J. and Dominguez, J. (2002), "Effects of space distribution of excitation on seismic response of arch dams", *J. Eng. Mech*, **128**(7), 759-768.

Mays, J.R., Dollar, D.A. and Roehm, L.H. (1989), "A concrete cracking analysis for the proposed arch raise of Roosevelt dam", *Comput. Struct.*, **32**(3/4), 679-689.

Olson, L.G. and Bathe, K.J. (1983), "A study of displacement-based fluid finite elements for calculating frequencies of fluid and fluid-structure systems", *Nucl. Eng. Des.*, **76**(2), 137-151.

Papaleontiou, C.G. and Tassoulas, J.L. (2012), "Evaluation of dam strength by finite element analysis", *Earthq. Struct.*, **3**(3), 457-471.

PEER: Pacific earthquake engineering research center (2015), http://ngawest2.berkeley.edu.

Perumalswami, P.R. and Kar, L. (1973), "Earthquake behavior of arch dams-reservoir systems", *Proceedings of the Fifth World Conference on Earthquake Engineering*, Rome.

Sohrabi-Gilani, M. and Ghaemian, M. (2012), "Spatial variation input effects on seismic response of arch dams", *Sci. Iranica*, **19**(4), 997-1004.

Szczesiak, T., Weber, B. and Bachmann, H. (1999), "Nonuniform earthquake input for arch dam-foundation interaction", *Soil Dy. Earthq. Eng.*, **18**(7), 487-493.

Tan, H. and Chopra, A.K. (1995a), "Earthquake analysis of arch dams including dam-water-foundation rock interaction", *Earthq. Eng. Struct. Dy.*, **24**(11), 1453-1474.

Tan, H. and Chopra, A.K. (1995b), "Dam-foundation rock interaction effects in frequency-response functions of arch dams", *Earthq. Eng. Struct. Dy.*, **24**(11), 1475-1489.

Valliappan, S., Yazdchi, M. and Khalili, N. (1999), "Seismic analysis of arch dams-a continuum damage mechanics approach", *Int. J. Numer. Method. Eng.*, **45**(11), 1695-1724.

Wang, J.T. and Chopra, A.K. (2010), "Linear analysis of concrete arch dams including dam-water-foundation rock interaction considering spatially-varying ground motions", *Earthq. Eng. Struct. Dy.*, **39**(7), 731-750.

Wang, J.T., Lv, D.D., Jin, F. and Zhang, C.H. (2013), "Earthquake damage analysis of arch dams considering dam–water–foundation interaction", *Soil Dy. Earthq. Eng.*, **49**, 64-74.

Wang, J.T., Zhang, C.H. and Jin, F. (2012), "Nonlinear earthquake analysis of high arch dam–water–foundation rock systems", *Earthq. Eng. Struct. Dy.*, **41**(7), 1157-1176.

Zienkiewicz, O.C. and Bettess, P. (1978), "Fluid-structure dynamic interaction and wave forces. An introduction to numerical treatment", *Int. J. Numer. Method. Eng.*, **13**(1), 1-16.

Zienkiewicz, O.C. and Taylor, R.L. (1989), *The finite element method*, **I**, Mc Graw-Hill.

CC